

Chiral density wave versus pion condensation in the 1+1 dimensional NJL model

Prabal Adhikari^{1,*} and Jens O. Andersen^{2,3,†}

¹*St. Olaf College, Physics Department, 1520 St. Olaf Avenue, Northfield, MN 55057, USA*

²*Department of Physics, Faculty of Natural Sciences,
NTNU, Norwegian University of Science and Technology,
Høgskoleringen 5, N-7491 Trondheim, Norway*

³*Niels Bohr International Academy, Blegdamsvej 17, Copenhagen 2100, Denmark*
(Dated: May 17, 2022)

In this paper, we study the possibility of an inhomogeneous quark condensate in the 1+1 dimensional Nambu-Jona-Lasinio model in the large- N_c limit at finite temperature T and quark chemical potential μ using dimensional regularization. The phase diagram in the μ - T plane is mapped out. At zero temperature, an inhomogeneous phase with a chiral-density wave exists for all values of $\mu > \mu_c$. Performing a Ginzburg-Landau analysis, we show that in the chiral limit, the critical point and the Lifschitz point coincide. We also consider the competition between a chiral-density wave and a constant pion condensate at finite isospin chemical potential μ_I . The phase diagram in the μ_I - μ plane is mapped out and shows a rich phase structure.

I. INTRODUCTION

Confinement and the spontaneous breaking of chiral symmetry are two of the most important properties of the QCD vacuum. The chiral condensate serves as an (approximate) order parameter for the chiral transition: At sufficiently high temperature or density, quarks are deconfined and chiral symmetry is at least partly restored. At asymptotically high temperature, QCD is a weakly interacting quark-gluon plasma, and at asymptotically high density, QCD is in the color-flavor locked phase and forms a color superconductor [1, 2]. At low temperature and high density, model calculations indicate that the chiral transition is of first order. This picture of a transition from a phase where chiral symmetry is broken by a homogeneous chiral condensate to a phase where chiral symmetry is (approximately) restored is probably too simplistic. Model calculations also suggest that there is an inhomogeneous phase for a small range of (low) temperatures and (high) densities. The idea of inhomogeneous phases at low temperature and high density dates back to the work by Fulde and Ferrell, and by Larkin and Ovchinnikov in the context of superconductors [3, 4], density waves in nuclear matter by Overhauser [5], and pion condensation by Migdal [6]. In recent years, inhomogeneous phases have been studied in, for example, cold atomic gases [7], color superconducting phases [8–10], quarkyonic phases [11, 12], as well as chiral condensates [13–24], see Refs. [25, 26] for recent reviews.

In order to solve the problem of inhomogeneous phases in its full generality, one must solve an infinite set of coupled gap equations for the various Fourier modes. This has not been done in three dimensions, but one hopes that a simple ansatz for the inhomogeneity will show many of the same features [26]. The inhomogeneities that have been considered in 3+1 dimensions are one-dimensional modulations such as chiral-density waves and soliton lattices.

Field theories in 1+1 dimensions have been studied extensively over the years as toy models for QCD since they share several important properties. For example, all Nambu-Jona-Lasinio (NJL) models in 1+1 dimensions are asymptotically free and show spontaneous breakdown of chiral symmetry in the vacuum with a dynamically generated mass scale. It should be pointed out, however, that in the NJL models in two dimensions the breakdown of a continuous symmetry only takes place in the large- N_c limit, since the phase fluctuations that would otherwise destroy a chiral condensate are of order $1/N_c$ [27, 28]. Although one is ultimately interested in 3+1 dimensions, the models in 1+1 dimensions are an ideal testing ground for new techniques. Calculations involving inhomogeneous phases can be found in [29–38]. One of the most important results in the past decade is the construction of the exact phase diagram of the massive Gross-Neveu model in the large- N_c limit [29, 30].

In Ref. [39], we investigated systematically different regularization schemes in effective models with inhomogeneous phases. The vacuum energy of the NJL model in 1+1 was calculated in the large- N_c limit in the background of a chiral-density wave. A naive application of for example momentum cutoff regularization or dimensional regularization leads to

* adhika1@stolaf.edu

† andersen@tf.phys.ntnu.no

an incorrect result for the vacuum energy. The problem is that there is a residual dependence on the wavevector b in the limit where the magnitude M goes to zero [35, 40]. This unphysical behavior can be remedied by subtracting the vacuum energy of the system in the normal phase after having performed a b -dependent unitary transformation on the Hamiltonian. We also showed that not all regulators are suited to perform a Ginzburg-Landau (GL) analysis of the critical and Lifschitz points; The proof of the equality of certain coefficients of the GL functional sometimes involves integration by parts and requires that the surface term vanishes. This is guaranteed if one uses dimensional regularization, but momentum cutoff regularization fails in certain cases, typically when the GL coefficients are divergent.

In this paper, we apply the techniques developed in Ref. [39] to map out the phase diagram in the μ - T plane both in and away from the chiral limit. We also consider the competition between a constant pion condensate and a chiral density wave at finite isospin. Our work is complementary to the study by Ebert et al [37], where the competition between a constant quark condensate and an inhomogeneous pion condensate was studied at $T = 0$ as a function of μ and μ_I .

The paper is organized as follows. In Sec. II, we briefly discuss the NJL model in 1+1 dimensions and we derive the thermodynamic potential at finite temperature and chemical potential using dimensional regularization. In Sec. III, we present the phase diagram and a Landau-Ginzburg analysis of the critical and Lifschitz points. In Sec. IV, we discuss the competition between the chiral density wave and a homogeneous pion condensate. Finally, in Sec. V we summarize our results. In appendix A, we provide the reader with some calculational details of two sum-integrals that are needed to locate the critical point and Lifschitz point.

II. LAGRANGIAN AND THERMODYNAMIC POTENTIAL

The Lagrangian of the NJL model in 1+1 dimensions is

$$\mathcal{L} = \bar{\psi} [i\rlap{\not{D}} - m_0 + (\mu + \frac{1}{2}\tau_3\mu_I)\gamma^0 - \sigma - i\gamma^5\pi_a\tau_a] \psi + \frac{G}{N_c} [(\bar{\psi}\psi)^2 + (\bar{\psi}i\gamma^5\tau\psi)^2] , \quad (1)$$

where N_c is the number of colors, τ_a are the three Pauli matrices ($a = 1, 2, 3$), m_0 is the current quark mass, Moreover ψ is a flavor doublet and a color

N_c -plet, and a two-component Dirac spinor. The γ -matrices are $\gamma^0 = \sigma_2$, $\gamma^1 = i\sigma_1$, and $\gamma^5 = \gamma^0\gamma^1 = \sigma_3$, where σ_i are the three Pauli matrices ($i = 1, 2, 3$). Here $\mu_B = 3\mu = \frac{3}{2}(\mu_u + \mu_d)$ is the baryon chemical potential and $\mu_I = \mu_u - \mu_d$ is the isospin chemical potential, where μ_f (with $f = u, d$) are the quark chemical potentials. The Lagrangian (1) is a generalization of the original Gross-Neveu model [41] which has a single quark flavor and a single quark chemical potential. The model (1) has a global $SU(N_c)$ symmetry and for $m_0 = \mu_I = 0$, it is also invariant under $SU_L(2) \times SU_R(2)$ transformations. For nonzero m_0 and $\mu_I = 0$, the latter symmetry is reduced to the group $SU_V(2)$. For $m_0 = 0$ and nonzero μ_I , it is reduced to $U_{I_3}(1) \times U_{AI_3}(1)$. For nonzero m_0 and μ_I , the symmetry is reduced to $U_{I_3}(1)$.

We next introduce the bosonic fields σ and π_a via

$$\sigma = -2\frac{G}{N_c}\bar{\psi}\psi , \quad (2)$$

$$\pi_a = -2\frac{G}{N_c}\bar{\psi}i\gamma^5\tau_a\psi . \quad (3)$$

The Lagrangian (1) then becomes

$$\mathcal{L} = \bar{\psi} [i\rlap{\not{D}} - m_0 + (\mu + \frac{1}{2}\tau_3\mu_I)\gamma^0 - \sigma - i\gamma^5\pi_a\tau_a] \psi - \frac{N_c(\sigma^2 + \pi_a^2)}{4G} . \quad (4)$$

The chiral condensate we choose is a chiral-density wave of the form

$$\langle\sigma\rangle = M \cos(2bz) - m_0 , \quad (5)$$

$$\langle\pi_3\rangle = M \sin(2bz) , \quad (6)$$

where b is a wavevector. For $b = 0$, it reduces to the standard homogeneous condensate. With a nonzero isospin chemical potential, there is also the possibility of a pion condensate Δ . For simplicity, we take this to be homogeneous

$$\langle\pi_1\rangle = \Delta . \quad (7)$$

The last term in Eq. (4) is denoted by $-V_0$, where V_0 is the tree-level potential. Inserting Eqs. (5)–(7) into V_0 and averaging over a volume L on the z -axis, we obtain

$$V_0 = N_c \frac{M^2 + m_0^2 - 2Mm_0\delta_{b,0} + \Delta^2}{4G} . \quad (8)$$

In the homogeneous case, the tree-level potential reduces to the standard expression $V_0 = N_c \frac{(M-m_0)^2 + \Delta^2}{4G}$.

The Dirac operator D can be written as

$$D = \bar{\psi} \left[i\rlap{\not{D}} + (\mu + \frac{1}{2}\tau_3\mu_I)\gamma^0 - Me^{2i\gamma^5\tau_3bz} - i\gamma^5\tau_1\Delta \right] \psi . \quad (9)$$

We next redefine the quark fields, $\psi \rightarrow e^{-i\gamma^5 \tau_3 b z} \psi$ and $\bar{\psi} \rightarrow \bar{\psi} e^{-i\gamma^5 \tau_3 b z}$, which corresponds to a unitary transformation of the Hamiltonian of the system. The Dirac operator then reads

$$D = [i\cancel{D} + \mu\gamma^0 + b'\tau_3\gamma^0 - M - i\gamma^5\tau_1\Delta] , \quad (10)$$

where $b' = (b + \frac{1}{2}\mu_I)$. Going to momentum space, Eq. (9) can be written as

$$D = [\cancel{p} + \mu\gamma^0 + b'\tau_3\gamma^0 - M - i\gamma^5\tau_1\Delta] . \quad (11)$$

Eq. (11) shows that the effective chemical potential for the u -quarks is $\mu + b' = \mu_u + b$, while for the d -quarks, it is $\mu - b' = \mu_d - b$. It is now straightforward to derive the fermionic spectrum in the background (6). It is given by the zeros of the Dirac determinant and reads [34, 35]

$$p_{0u} = E_{\Delta}^- - \mu , \quad p_{0d} = E_{\Delta}^+ - \mu , \quad (12)$$

$$p_{0\bar{u}} = -(E_{\Delta}^+ - \mu) , \quad p_{0\bar{d}} = -(E_{\Delta}^- - \mu) , \quad (13)$$

where

$$E_{\Delta}^{\pm} = \sqrt{E_{\pm}^2 + \Delta^2} , \quad E_{\pm} = \sqrt{p^2 + M^2} \pm b' . \quad (14)$$

We note that the spectrum depends on the isospin chemical potential μ_I via b' . Having derived the spectrum, the one-loop contribution to the thermodynamic potential is given by

$$V_1 = -N_c \oint_{\{P\}} \log [P_0^2 + (E_{\Delta}^{\pm})^2] , \quad (15)$$

where the sum-integral is defined by

$$\oint_{\{P\}} = \left(\frac{e^{\gamma_E \Lambda^2}}{4\pi} \right)^{\epsilon} T \sum_{\{P_0\}} \int \frac{d^d p}{(2\pi)^d} , \quad (16)$$

where $d = 1 - 2\epsilon$ and Λ is the renormalization scale associated with the $\overline{\text{MS}}$ scheme. $P_0 = (2n+1)\pi T + \mu$ are the fermionic Matsubara frequencies with $n = 0, \pm 1, \pm 2, \dots$. Summing over the Matsubara frequencies, we can write

$$V_1 = -N_c \int_p \left\{ E_{\Delta}^{\pm} + T \log \left[1 + e^{-\beta(E_{\Delta}^{\pm} - \mu)} \right] + T \log \left[1 + e^{-\beta(E_{\Delta}^{\pm} + \mu)} \right] \right\} . \quad (17)$$

The first term in Eq. (17) is ultraviolet divergent and requires regularization. The two contributions from E_{Δ}^{\pm} to this term are denoted by V_{\pm}^{vac} . The second and third term which depend on the temperature and the chemical potential are finite.

After integrating over angles and changing variables, $u = \sqrt{p^2 + M^2}$, we can write

$$V_{\pm}^{\text{vac}} = -\frac{N_c (e^{\gamma_E \Lambda^2})^{\epsilon}}{\sqrt{\pi} \Gamma(\frac{1}{2} - \epsilon)} \int_M^{\infty} \sqrt{(u \pm b')^2 + \Delta^2} \times \frac{u du}{(u^2 - M^2)^{\frac{1}{2} + \epsilon}} . \quad (18)$$

We cannot calculate analytically the vacuum energy for nonzero Δ . In order to isolate the divergences, we expand the dispersion relations around $u = \infty$ and find appropriate subtraction terms. We can then write

$$V_{\pm}^{\text{vac}} = V_{\text{div}\pm}^{\text{vac}} + V_{\text{fin}\pm}^{\text{vac}} , \quad (19)$$

where

$$V_{\text{div}\pm}^{\text{vac}} = -\frac{N_c (e^{\gamma_E \Lambda^2})^{\epsilon}}{\sqrt{\pi} \Gamma(\frac{1}{2} - \epsilon)} \left[\int_M^{\infty} |u \pm b'| + \frac{\Delta^2}{2u} \right] \frac{u du}{(u^2 - M^2)^{\frac{1}{2} + \epsilon}} , \quad (20)$$

$$V_{\text{fin}\pm}^{\text{vac}} = -\frac{N_c (e^{\gamma_E \Lambda^2})^{\epsilon}}{\sqrt{\pi} \Gamma(\frac{1}{2} - \epsilon)} \int_M^{\infty} \left[E_{\Delta}^{\pm} - |u \pm b'| - \frac{\Delta^2}{2u} \right] \frac{u du}{(u^2 - M^2)^{\frac{1}{2} + \epsilon}} . \quad (21)$$

We denote the sum of the two terms in (21) by $V_{\text{fin}}^{\text{vac}}(M, \Delta, b')$. Note that $V_{\text{fin}\pm}^{\text{vac}}(M, 0, b') = 0$. In the chiral limit, the solutions to the gap equations are $M \neq 0$ and $\Delta = 0$ or $M = 0$ and $\Delta \neq 0$. In the latter case, Eqs. (20) and (21) both have infrared divergences. The IR divergences of (20) cancel against those of (21). However, they must be regulated separately, which is inconvenient. See also Appendix A.

$V_{\text{div}\pm}^{\text{vac}}$ can now be calculated using dimensional regularization and the result is

$$V_{\text{div}\pm}^{\text{vac}} = \frac{N_c}{4\pi} \left(\frac{e^{\gamma_E \Lambda^2}}{M^2} \right)^{\epsilon} [M^2 \Gamma(-1 + \epsilon) - \Delta^2 \Gamma(\epsilon)] + \theta(b' - M) f(M, b') , \quad (22)$$

where the function $f(M, b')$ is defined by

$$f(M, b) = -\frac{N_c}{\pi} \left[b' \sqrt{b'^2 - M^2} - M^2 \log \frac{b' + \sqrt{b'^2 - M^2}}{M} \right] \quad (23)$$

The contribution $V_{\text{div}+}^{\text{vac}}$ to the vacuum energy is independent of b , while the extra term $f(M, b')$ in $V_{\text{div}-}^{\text{vac}}$ arises from the integral $\int_M^\infty |u - b'|$ where one must distinguish between $u < b'$ and $u > b'$.

Expanding $V_{\text{div}}^{\text{vac}} = V_{\text{div}+}^{\text{vac}} + V_{\text{div}-}^{\text{vac}}$ in powers of ϵ , we find

$$V_{\text{div}} = -\frac{N_c}{2\pi} \left(\frac{\Lambda^2}{M^2} \right)^\epsilon \left[M^2 \left(\frac{1}{\epsilon} + 1 \right) + \Delta^2 \frac{1}{\epsilon} \right] + \theta(b' - M) f(M, b'). \quad (24)$$

As explained in introduction, one must subtract the vacuum energy for the system in the normal state (after a unitary transformation) in order to obtain a result that is independent of b in the limit $M \rightarrow 0$. Thus we must subtract the term

$$V_{\text{div}}^{\text{sub}} = -\frac{N_c}{2\pi} \left(\frac{\Lambda^2}{m_0^2} \right)^\epsilon m_0^2 \left(\frac{1}{\epsilon} + 1 \right) + \theta(b' - m_0) f(m_0, b'), \quad (25)$$

where we have used that $V_{\text{fin}}^{\text{sub}}(m_0, 0, b) = 0$. Eq. (24) contains poles in ϵ and they are removed by the renormalization of the coupling constant G and the fermion mass m_0 making the substitutions

$$\frac{1}{G} \rightarrow \frac{1}{G} \left[1 + \frac{2G}{\pi\epsilon} \right], \quad (26)$$

$$m_0 \rightarrow m_0 \left[1 + \frac{2G}{\pi\epsilon} \right]^{-1}. \quad (27)$$

Note in particular that the ratio $\frac{m_0}{G}$ is the same for bare and renormalized quantities. After renormalization, making the substitutions Eqs. (26) and (27), the vacuum energy $V = V_0 + V_1$ becomes

$$V = N_c \frac{(M^2 + m_0^2 - 2Mm_0\delta_{b,0}) + \Delta^2}{4G} - \frac{N_c M^2}{2\pi} \left[\log \frac{\Lambda^2}{M^2} + 1 \right] - \frac{N_c \Delta^2}{2\pi} \log \frac{\Lambda^2}{M^2} + V_{\text{fin}}^{\text{vac}} + \theta(b' - M) f(M, b') - \theta(b' - m_0) f(m_0, b') + \theta(\tfrac{1}{2}\mu_I - m_0) f(m_0, \tfrac{1}{2}\mu_I), \quad (28)$$

where we kept only the b' -dependent term from Eq. (25). Note also that we added the term $\theta(\tfrac{1}{2}\mu_I - m_0) f(m_0, \tfrac{1}{2}\mu_I)$. This term is necessary in order to get the correct expression for the isospin density n_I in the limit $b \rightarrow 0$ [34]. In Appendix A, we show that the vacuum energy (28) is independent of b in the limit $M \rightarrow 0$.

The coupling constant G and the mass parameter m_0 satisfy the renormalization group equations

$$\Lambda \frac{dG}{d\Lambda} = -\frac{4G^2}{\pi}, \quad (29)$$

$$\Lambda \frac{dm_0}{d\Lambda} = -\frac{4m_0 G}{\pi}. \quad (30)$$

The solutions are

$$G(\Lambda) = \frac{G_0}{1 + \frac{4}{\pi} G_0 \log \frac{\Lambda}{\Lambda_0}}, \quad (31)$$

$$m_0(\Lambda) = m_0(\Lambda_0) G(\Lambda), \quad (32)$$

where $G_0 = G(\Lambda_0)$ and Λ_0 is some reference scale. These equations show that the ratio $\frac{m_0}{G}$ is independent of the scale Λ . We also note that $G(\Lambda)$ decreases with Λ showing that the model is asymptotically free.

In the vacuum, we have $\Delta = b = 0$. With vanishing isospin chemical potential μ_I and in the chiral limit, the solutions M_0 to the gap equation $\frac{dV}{dM} = 0$ are either $M_0 = 0$ or

$$M_0 = \Lambda e^{-\frac{\pi}{4G}}. \quad (33)$$

Using Eq. (29), it is straightforward to verify that M_0 is independent of the renormalization scale Λ . The nonanalytic behavior of M_0 as a function of G shows that the result is nonperturbative. Using for example the two-particle irreducible action formalism, it can be shown that this result corresponds the summation of the daisy and superdaisy graphs from all orders of perturbation theory [42, 43]. We

can trade the scale Λ for the scale M_0 , which gives

$$V = -\frac{N_c M^2}{2\pi} \left[\log \left(\frac{M_0^2}{M^2} \right) + 1 \right], \quad (34)$$

in agreement with Ebert et al [35]. It is easy to see that the global minimum of V is at $M = M_0$. In the remainder of this paper, we express all dimensionful quantities in appropriate powers of the dynamically generated mass scale M_0 .

The finite-temperature term is the second and third term from (17),

$$V^T = -\frac{N_c T}{\pi} \int_0^\infty \left\{ \log \left[1 + e^{-\beta(E_\Delta^\pm - \mu)} \right] + \log \left[1 + e^{-\beta(E_\Delta^\pm + \mu)} \right] \right\} dp. \quad (35)$$

The complete free energy in the large- N_c limit is then given by the sum of Eq. (28) and Eq. (35). In contrast to 3+1 dimensions, we have no experimental input that allows us to determine the constituent

quark mass m_0 appearing in the expression for the free energy. Following Ref. [34], we demand that the ratio of the dynamical quark mass M and the pion mass m_π be the same as in three dimensions for $\mu = \mu_I = 0$. Choosing the values $M = 350$ MeV and $m_\pi = 140$ MeV, one finds a ratio $\frac{M}{m_\pi} = \frac{5}{2}$. Numerically, this corresponds to values $m_0 = 0.05M_0$, $M = 1.04M_0$, and $m_\pi = 0.42M_0$, where M_0 is the dynamical quark mass for $m_0 = 0$. Introducing the dimensionless $\alpha = \pi \frac{m_0}{M_0}$, this corresponds to $\alpha = 0.17$. In the remainder of the paper, we use this value for α . Moreover, since all contributions to the effective potential and gap equations are proportional to N_c , we omit this factor in all the numerical work.

III. CHIRAL-DENSITY WAVE AND NO PION CONDENSATE

In the absence of a pion condensate, the vacuum energy (28) reduces to

$$V = N_c \frac{(M^2 + m_0^2 - 2Mm_0\delta_{b,0})}{4G} - \frac{N_c M^2}{2\pi} \left[\log \frac{\Lambda^2}{M^2} + 1 \right] + \theta(b' - M)f(M, b') - \theta(b' - m_0)f(m_0, b') + \theta(\frac{1}{2}\mu_I - m_0)f(m_0, \frac{1}{2}\mu_I). \quad (36)$$

The finite-temperature term is given by Eq. (35) evaluated for $\Delta = 0$.

A. Zero temperature

In the limit $T \rightarrow 0$ and for vanishing pion condensate, $\Delta = 0$, one can obtain analytic results for the density-dependent contributions to the effective potential given by Eq. (35). The contributions from the first Eq. (35) are denoted by V_\pm^{med} . After integrating over angles, we find

$$V_\pm^{\text{med}} = -\frac{N_c}{\pi} \int_0^\infty (\mu - E_\pm) \theta(\mu - E_\pm) dp. \quad (37)$$

The contributions from the second line of Eq. (35) are denoted by $V_\pm^{0,\text{med}}$ and given by the substitution $M \rightarrow m_0$ in (37). The contribution V_+^{med} is straightforward to compute. After changing variables $u = \sqrt{p^2 + M^2}$ and noting that the upper limit is $u_f = \mu - b$ due to the step function, we find

$$\begin{aligned} V_+^{\text{med}} &= -\frac{N_c}{\pi} \int_M^{u_f} \frac{du u}{\sqrt{u^2 - M^2}} (\mu - u - b') \\ &= -\frac{N_c}{2\pi} \left[(\mu - b') \sqrt{(\mu - b')^2 - M^2} - M^2 \log \frac{\mu - b' + \sqrt{(\mu - b')^2 - M^2}}{M} \right] \theta(\mu - b' - M). \end{aligned} \quad (38)$$

We next consider the contribution V_-^{med} , which is given by

$$V_-^{\text{med}} = -\frac{N_c}{\pi} \int_0^\infty (\mu - E_-) \theta(\mu - E_-) dp. \quad (39)$$

Here we must distinguish between several cases.

1. $M > b'$. The dispersion relation is shown in the left panel of Fig. 1. In this case $E_- = \sqrt{p^2 + M^2} - b'$. After changing variables $u = \sqrt{p^2 + M^2}$, the integral then becomes

$$V_-^{\text{med}} = -\frac{N_c}{\pi} \int_M^{u_f} \frac{du u}{\sqrt{u^2 - M^2}} (\mu - u + b'), \quad (40)$$

where $u_f = \mu + b'$ and $\mu > M - b'$. This yields

$$V_-^{\text{med}} = -\frac{N_c}{2\pi} \left[(\mu + b') \sqrt{(\mu + b')^2 - M^2} - M^2 \log \frac{\mu + b' + \sqrt{(\mu + b')^2 - M^2}}{M} \right] \theta(\mu + b' - M). \quad (41)$$

This contribution is obtained from (38) by the substitution $b' \rightarrow -b'$.

2. $b' > M$. The dispersion relation is shown in the right panel of Fig. 1 (blue curve). In this case $E_- = b' - \sqrt{p^2 + M^2}$ for $u < b'$ or $E_- = \sqrt{p^2 + M^2} - b'$ for $u > b'$.

- (a) If $\mu > b' - M$, the integration is from $p = 0$ to $p_C = p_f = \sqrt{(b' + \mu)^2 - M^2}$ or $u = M$ to $u = u_f = \mu + b'$. The green horizontal line indicates the value of the chemical potential and the intersection with the dispersion relation gives the upper limit of integration. This yields

$$V_-^{\text{med}} = -\frac{N_c}{\pi} \left[\frac{1}{2} (\mu + b') \sqrt{(b' + \mu)^2 - M^2} - b' \sqrt{b'^2 - M^2} + M^2 \log \frac{b' + \sqrt{b'^2 - M^2}}{M} - \frac{1}{2} M^2 \log \frac{b' + \mu + \sqrt{(b' + \mu)^2 - M^2}}{M} \right] \theta(\mu - b' + M). \quad (42)$$

- (b) If $\mu < b' - M$, the integration is from $p_A = \sqrt{(b' - \mu)^2 - M^2}$ to $p_B = p_f = \sqrt{(b' + \mu)^2 - M^2}$ or $u = b' - \mu$ to $u = b' + \mu$. The value of the chemical potential is indicated by the orange line and the intersection with the dispersion relation gives the upper and lower limits of integration. This gives

$$V_-^{\text{med}} = -\frac{N_c}{\pi} \left[\frac{1}{2} (b' + \mu) \sqrt{(b' + \mu)^2 - M^2} + \frac{1}{2} (b' - \mu) \sqrt{(b' - \mu)^2 - M^2} - b' \sqrt{b'^2 - M^2} - \frac{1}{2} M^2 \log \frac{b' + \mu + \sqrt{(b' + \mu)^2 - M^2}}{b' + \sqrt{b'^2 - M^2}} - \frac{1}{2} M^2 \log \frac{b' - \mu + \sqrt{(b' - \mu)^2 - M^2}}{b' + \sqrt{b'^2 - M^2}} \right] \theta(b' - M - \mu). \quad (43)$$

The result for the full effective potential in the large- N_c limit, first found in Ref. [35]

$$V = -\frac{N_c M^2}{2\pi} \left[\log \frac{M^2}{M_0^2} + 1 \right] - \theta(b' - m_0) f(m_0, b') + \theta(\frac{1}{2}\mu_I - m_0) f(m_0, \frac{1}{2}\mu_I) - \frac{N_c}{2\pi} \left[(\mu + b') \sqrt{(\mu + b')^2 - M^2} - M^2 \log \frac{\mu + b' + \sqrt{(\mu + b')^2 - M^2}}{M} \right] \theta(\mu + b' - M) - \frac{N_c}{2\pi} \left[|\mu - b'| \sqrt{(\mu - b')^2 - M^2} - M^2 \log \frac{|\mu - b'| + \sqrt{(\mu - b')^2 - M^2}}{M} \right] \theta(|\mu - b'| - M). \quad (44)$$

In Fig. 2, we show the magnitude M (blue solid line) and the wavevector b (red dashed line) both normalized to M_0 as functions of the chemical potential μ at $\mu_I = T = 0$. The transition from a constant chiral condensate to a condensate with a nonzero

wavevector b is first order. In the chiral limit, this phase extends to all values of the chemical potential [35]. Away from the chiral limit, there is a transition from the phase with a chiral density wave to a chirally symmetric phase at finite μ , which is also first

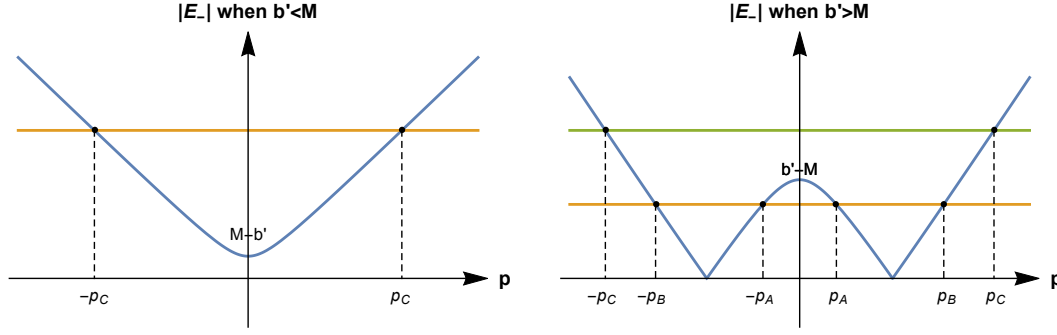


FIG. 1. (Color online) Dispersion relation E_- for $\Delta = 0$ (blue curve) for $b' < M$ (left panel) and for $b' > M$ (right panel). The horizontal green line is for the case $\mu > b' - M$ and the horizontal orange line is for the case $\mu < b' - M$. See main text for discussion of the regions of integration in the different cases.

order.

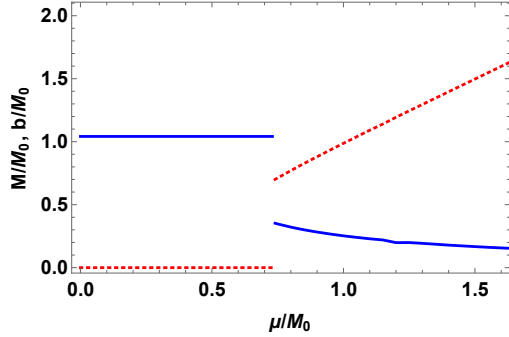


FIG. 2. (Color online) Normalized magnitude of the quark condensate M/M_0 (blue solid line) and wavevector b/M_0 (red dashed line) as functions of μ/M_0 at $\mu_I = T = 0$ away from the chiral limit.

Since $b = b(\mu)$ is larger than $M = M(\mu)$ in the inhomogeneous phase, it is clear that dispersion relation for the u -quarks is that shown in the right panel of Fig. 1. This implies that the energy of a u -quark is zero for the finite momentum $p_{\min} = \sqrt{b^2 - M^2}$. This is contrast to the d -quarks, which are always gapped with a gap $M + b$.

B. Finite temperature

The complete finite-temperature effective potential is given by the sum of the vacuum term (28) and Eq. (35). In Fig. 3, we show the phase diagram in the chiral limit. This phase diagram was first obtained by Ebert et al [35]. The dashed black and red lines indicate a second-order transition, while the solid red

line indicates a first-order transition. Note that the phase with nonzero M and b extends to infinity for $T = 0$. The black dot shows the position of the Lifshitz point whose coordinates will be given below. The black solid line indicates the first-order transition in the homogeneous case. The critical point for this transition coincides with the tricritical point as will be shown below.

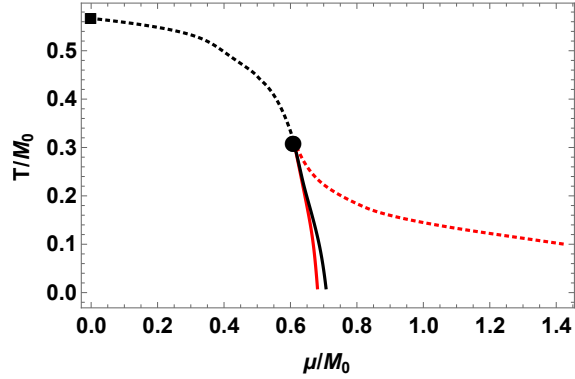


FIG. 3. (Color online) Phase diagram in the chiral limit. The dashed black and red lines indicates a second-order transition, while the red solid line indicates a first-order transition. The black dot indicates the tricritical point which coincides with the critical end point. The solid black line is the first order transition in the homogeneous case.

In Fig. 4, we show the phase diagram away from the chiral limit. In contrast to case $m_0 = 0$, the phase with nonzero M and b has finite extent. Both transitions from and to the symmetric phase are first

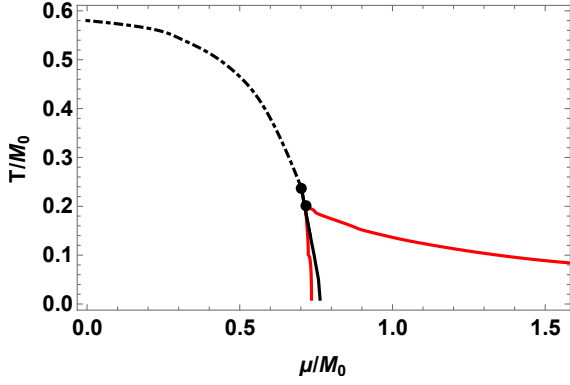


FIG. 4. (Color online) Phase diagram away from the chiral limit. The dashed-dotted line is a crossover and the solid line is a first-order transition. The black dots indicate the critical end point and the tricritical point.

order. We also note that the critical end point and the tricritical point do not coincide, in contrast to the result in the chiral limit. In the chiral limit, the position of the critical end point and the tricritical point can also be found from a Ginzburg-Landau analysis. We then expand the effective potential in powers of M and derivatives. In the chiral limit, the first few terms of this expansion are

$$V = \frac{N_c M^2}{4G} - 2N_c M^2 \sum_{\{P\}} \frac{1}{P^2} + N_c M^4 \sum_{\{P\}} \frac{1}{P^4} - \frac{1}{3} N_c (\nabla M)^2 \sum_{\{P\}} \frac{p^2 - 3P_0^2}{P^6}. \quad (45)$$

We denote by β_1 , β_2 and β_3 the coefficients of M^2 , M^4 and $(\nabla M)^2$, respectively. It is easy to show by direct integration over p or by partial integration, that the coefficients β_2 and β_3 are equal. The coefficients are equal also if one uses momentum cutoff regularization. This is in contrast to three dimensions where only dimensional regularization [39] or Pauli-Villars regularization [15] yield $\beta_2 = \beta_3$ due to the absence of surface terms. The critical point is given by the condition that the quadratic and quartic terms vanish, and the Lifschitz point is given by the condition that the quadratic and gradient terms vanish. The equality of β_2 and β_3 implies that the critical point and the Lifschitz point coincide. The condition that these coefficients vanish implies the coupled equations

$$\frac{1}{8G} - \sum_{\{P\}} \frac{1}{P^2} = 0, \quad (46)$$

$$\sum_{\{P\}} \frac{1}{P^4} = 0. \quad (47)$$

The coefficients β_i ($i = 1, 2, 3$) are all infrared safe since all the fermionic Matsubara frequencies are nonzero. If one separates the sum-integrals in a vacuum term and a term that depends on T and μ , they are both divergent in the infrared, but these divergences cancel in the sum. The sum-integral $\sum_{\{P\}} \frac{1}{P^2}$ is also UV divergent and in Eq. (46) needs to be renormalized. The sum-integrals appearing in Eqs. (46)–(47) are calculated in Appendix A. Using the expression (A7) and the substitution (26), the renormalized version of Eq. (46) can be written as

$$\frac{1}{8G} - \frac{1}{2\pi} \left[\log \frac{\Lambda}{T} + \gamma_E - \log 2 + \frac{\partial \text{Li}_{-2\epsilon_{\text{IR}}}(-e^{-\beta\mu})}{\epsilon_{\text{IR}}} \Big|_{\epsilon_{\text{IR}}=0} + \frac{\partial \text{Li}_{-2\epsilon_{\text{IR}}}(-e^{\beta\mu})}{\epsilon_{\text{IR}}} \Big|_{\epsilon_{\text{IR}}=0} \right] = 0, \quad (48)$$

where we have used $\Lambda = \Lambda_{\text{UV}}$ and $\epsilon = \epsilon_{\text{UV}}$. Using Eq. (33), we can trade G for M_0 and Eq. (48) can be written as

$$\frac{1}{2\pi} \left[\log \frac{M_0}{T} + \gamma_E - \log 2 + \frac{\partial \text{Li}_{-2\epsilon_{\text{IR}}}(-e^{-\beta\mu})}{\epsilon_{\text{IR}}} \Big|_{\epsilon_{\text{IR}}=0} + \frac{\partial \text{Li}_{-2\epsilon_{\text{IR}}}(-e^{\beta\mu})}{\epsilon_{\text{IR}}} \Big|_{\epsilon_{\text{IR}}=0} \right] = 0. \quad (49)$$

Using Eq. (A10), Eq. (47) can be conveniently written as

$$\frac{1}{32\pi^2 T^3} [\psi(\frac{1}{2} + \frac{i\mu}{2\pi T}) + \psi(\frac{1}{2} - \frac{i\mu}{2\pi T})] = 0. \quad (50)$$

The solution to Eqs. (49) and (50) gives the position of the Lifschitz point in the μ - T plane. The solution is $(\mu/M_0, T/M_0) = (0.6082, 0.3183)$ and equals the

critical point in the chiral limit. The position agrees with the numerical result from the phase diagram shown in Fig. 3. In the same manner we can find the critical temperature for the transition at $\mu = 0$. Eq. (49) reduces to

$$\frac{1}{2\pi} \left[\log \frac{M_0}{\pi T} + \gamma_E \right] = 0, \quad (51)$$

whose solution is $\frac{T}{M_0} = \frac{e^{\gamma E}}{\pi} \approx 0.567$. The point $(0.567, 0)$ is also marked with a black square in Fig. 3.

IV. CHIRAL-DENSITY WAVE VERSUS HOMOGENEOUS PION CONDENSATE

In this section, we include the possibility of a constant pion condensate. A constant pion condensate will form at $T = 0$ once the isospin chemical potential exceeds the mass of the pion.

A. Zero temperature

In Fig. 5, we show the normalized quark and pion condensates as functions of the isospin chemical potential at zero baryon chemical potential and at zero temperature. For $\mu = 0$, the wavevector b vanishes. The pions condense at the $\mu_I = m_\pi$ which in units of M_0 is approximately 0.42. Once the pion condensate starts increasing, the quark condensate decreases and one can think of this as a rotation of the quark condensate into a pion condensate as μ_I increases. In the chiral limit, the pion condensate forms for μ_I infinitesimally larger than zero and the quark condensate vanishes identically [37]. More generally, in the chiral limit, there is no solution to the gap equations with $M \neq 0$ and $\Delta \neq 0$ simultaneously [37].

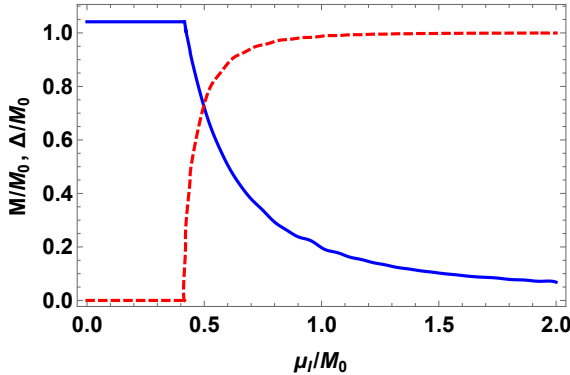


FIG. 5. (Color online) Normalized quark M/M_0 (blue solid line) and pion condensates Δ/M_0 (red dashed line) as functions of μ_I/M_0 at $\mu = T = 0$.

In the left panel of Fig. 7, we show the condensate M/M_0 as a function of μ_I/M_0 for $\mu/M_0 = 0.9$ in the homogeneous case, i.e. we do not allow for a nonzero wavevector b . The two transitions are of first order. In the right panel of Fig. 7, we show the condensate M/M_0 and b/M_0 as functions of μ_I/M_0 for $\mu/M_0 = 0.9$ in the inhomogeneous case, i.e. we allow for a nonzero wavevector b . The two transitions are of first order.

The region in the μ - μ_I plane where $M = M_0$ and $\Delta = b = 0$ is the vacuum. In this region it can be shown by taking appropriate derivatives of the partition function, that physical quantities are independent of the chemical potentials μ and μ_I . This is an example of the silver blaze property [44].

In Fig. 6, we show the phase diagram for nonzero quark masses in the μ_I - μ plane at $T = 0$. The values of M , b , and Δ are shown for the different regions. The transition from the vacuum phase to the phase with a homogeneous pion condensate is second order. The other transitions are all first order with a jump in the value of M and possibly a jump in the value of b .

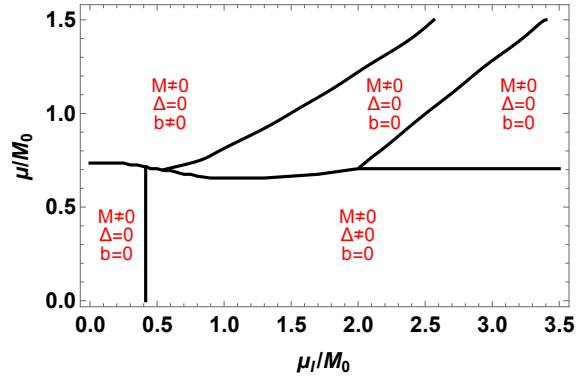


FIG. 6. (Color online) Phase diagram away from the chiral limit in the μ_I - μ plane at $T = 0$. See main text for details.

This phase diagram generalizes Fig. 5 of Ref. [34] in which only constant condensates were considered. The phase with $M \neq 0$ and $b \neq 0$ for large values of μ and small values of μ_I replaces the phase with a constant chiral condensate.

As mentioned above, in the chiral limit, the pion condensate forms for μ_I infinitesimally small. Thus the vacuum phase with $M \neq 0$ and $b = \Delta = 0$ reduces to a line along the μ -axis.

This plot corresponds to a horizontal line in Fig. 6 with $\mu/M_0 = 0.9$.

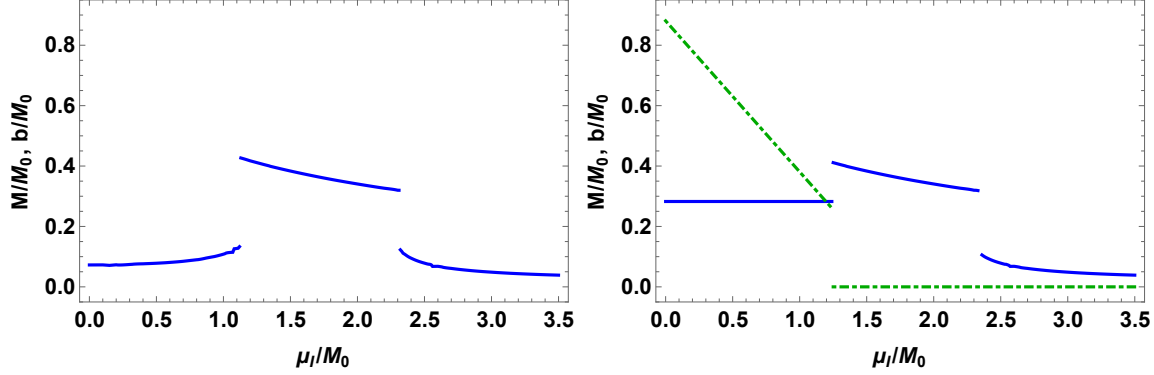


FIG. 7. (Color online) Left panel: Normalized quark condensate M/M_0 at $T = 0$ as function of μ_I/M_0 for $\mu/M_0 = 0.9$ for $b = 0$. Right panel: Normalized magnitude of the quark condensate M/M_0 (blue line) and wavevector b/M_0 (green line) at $T = 0$ as functions of μ_I/M_0 for $\mu/M_0 = 0.9$.

Let us finally discuss the quark and isospin densities in the different phases. These are given by

$$n_q = -\frac{\partial V}{\partial \mu}, \quad n_I = -\frac{\partial V}{\partial \mu_I}, \quad (52)$$

where $V = V_0 + V_1$ is the full zero-temperature effective potential. In the phases, where $\Delta = 0$, these expressions can be obtained by differentiation of Eq. (44). This yields

$$n_q = \frac{N_c}{\pi} \sqrt{(\mu + b')^2 - M^2} \theta(\mu + b' - M) + \frac{N_c}{\pi} \sqrt{(\mu - b')^2 - M^2} \theta(|\mu - b'| - M) \text{sign}(\mu - b'), \quad (53)$$

$$n_I = \frac{N_c}{2\pi} \sqrt{(\mu + b')^2 - M^2} \theta(\mu + b' - M) - \frac{N_c}{2\pi} \sqrt{(\mu - b')^2 - M^2} \theta(|\mu - b'| - M) \text{sign}(\mu - b') \\ - \frac{N_c}{\pi} \sqrt{b'^2 - m_0^2} \theta(b' - m_0) + \frac{N_c}{\pi} \sqrt{\frac{1}{4}\mu_I^2 - m_0^2} \theta(\frac{1}{2}\mu_I - m_0). \quad (54)$$

In the vacuum phase, $b = 0$ and so $b' = \frac{1}{2}\mu_I$. Moreover, $M > \mu + \frac{1}{2}\mu_I$ and so $n_q = n_I = 0$. This reflects the silver blaze property of the vacuum, namely that its properties are independent of the chemical potential(s) up to some critical value(s) above which there is a phase transition. In the pion-condensed phase, one cannot find a simple analytic expressions for n_q and n_I . However, from (52) and the zero-temperature limit of Eq. (17), one finds [34]

$$n_q = \frac{N_c}{\pi} \int_0^\infty [\theta(\mu - E_\Delta^+) + \theta(\mu - E_\Delta^-)] dp, \quad (55)$$

$$n_I = \frac{N_c}{2\pi} \int_0^\infty \left[\frac{E_\Delta^+}{E_\Delta^+} \theta(\mu - E_\Delta^+) - \frac{E_\Delta^-}{E_\Delta^-} \theta(\mu - E_\Delta^-) \right] dp. \quad (56)$$

Since $E_\Delta^\pm > 0$ in this phase, we immediately obtain $n_q = 0$ and $n_I \neq 0$.

B. Finite temperature

In Fig. 8, we show the phase diagram for finite quark masses in the μ_I - μ -plane for $T/M_0 = 0.01$. The inhomogeneous phase now has become an island which shrinks as the temperature increases further and eventually disappears. The chiral condensate M is continuous through the corridor. The transitions are all of first order. The two phases with $M \neq 0$ and $b = \Delta = 0$ in the upper right part of Fig. 6 have now merged to a single phase.

In Fig. 9, we show the normalized quark condensate M/M_0 and wavevector b/M_0 as functions of μ/M_0 for $\mu_I = 0$ and $T/M_0 = 0.1$. The two transitions are first order.

In Fig. 10, we show the normalized quark condensate M/M_0 as a function of μ_I/M_0 for $\mu/M_0 = 0.9$ and $T/M_0 = 0.01$ with the restriction of a constant

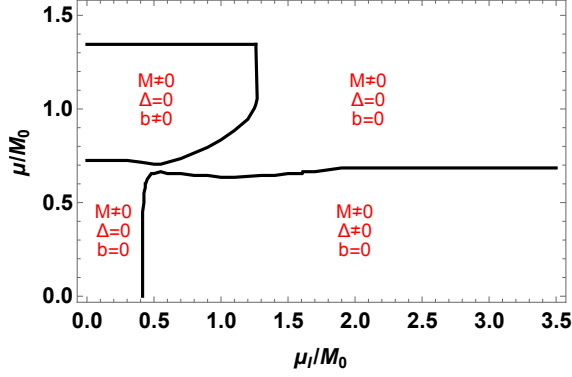


FIG. 8. (Color online) Phase diagram away from the chiral limit in the μ_I - μ plane for $T/M_0 = 0.01$. See main text for details.

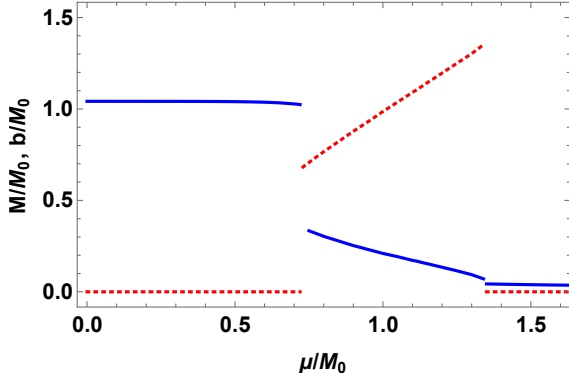


FIG. 9. (Color online) Normalized quark condensate M/M_0 and wavevector b/M_0 as functions of μ/M_0 for $\mu_I = 0$ and $T/M_0 = 0.1$.

condensate i.e. for $b = 0$. In contrast to the case at $T = 0$, cf. Fig. 7, M/M_0 is continuous.

In Fig. 11, we show the normalized quark condensate M/M_0 (blue line) and b/M_0 (green line) as functions of μ_I/M_0 for $\mu/M_0 = 0.9$ and $T/M_0 = 0.01$. M/M_0 is discontinuous only for one value of μ_I showing that the the phases with $M/M_0 \neq 0$ and $b = \Delta = 0$ have merged to a single phase, cf. the upper right part of Fig. 8.

V. SUMMARY

In this paper, we have studied aspects of the phase diagram of the NJL model in 1+1 dimensions in the large- N_c limit as a function of T , μ , and μ_I using dimensional regularization. The calculations are done

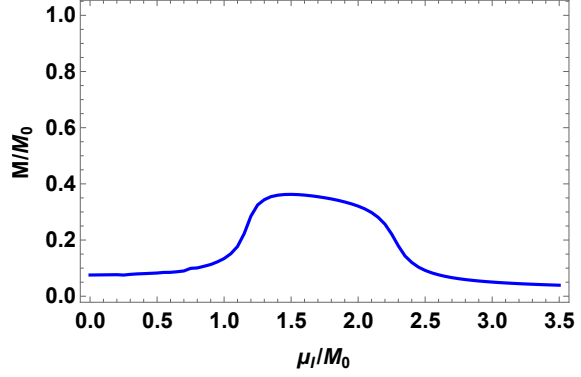


FIG. 10. (Color online) Normalized chiral condensate M/M_0 as a function of μ_I/M_0 for $\mu/M_0 = 0.9$ and $T/M_0 = 0.01$ in the homogeneous case, i.e. we do not allow for nonzero b .

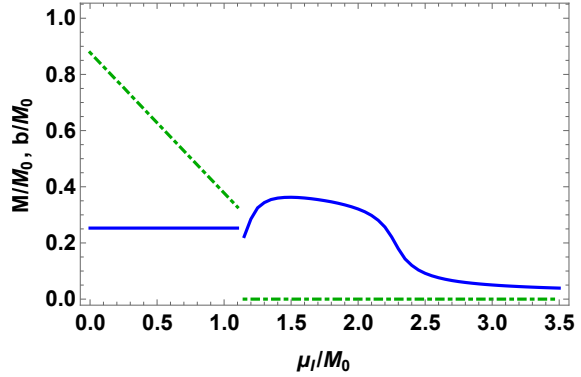


FIG. 11. (Color online) Normalized chiral condensate M/M_0 (blue line) and wavevector b/M_0 (green line) as functions of μ_I/M_0 for $\mu/M_0 = 0.9$ and $T/M_0 = 0.01$.

with finite quark masses and generalize the results of [34] in which only homogeneous condensates were considered.

We have also carried out a GL analysis of the critical and the Lifschitz points and derived a set of equations that determine their position in the μ - T plane. In the chiral limit they coincide, while they are separated away from it, cf. Figs. 3 and 4. Dimensional regularization proved to be very useful in their calculation since it can be conveniently used to regulate infrared divergences at intermediate steps, which cancel in the final result.

In this paper, we restricted ourselves to a constant pion condensate. The related problem of a constant chiral condensate and an inhomogeneous pion condensate was considered in Ref. [37]. It would be of

interest to extend our calculations to allow for spatially modulated chiral and pion condensates at the same time. Eq. (7) would then be replaced by

$$\langle \pi_1 \rangle = \Delta \cos(2kz), \quad \langle \pi_2 \rangle = \Delta \sin(2kz), \quad (57)$$

where k is another wavevector. One complication that arises in the case of an inhomogeneous pion condensate is that one can no longer find an analytic expressions for the dispersion relations, but they must be solved numerically. Some work along these lines in the chiral limit has been done by Ebert et al [37], but a complete mapping of the phase diagram with nonzero quark masses is still missing.

ACKNOWLEDGMENTS

The authors would like to thank the Niels Bohr International Academy for its hospitality. P.A. would like to acknowledge the research travel support provided by the Office of the Dean and the Physics Department at St. Olaf College. P.A. would also like to thank Professor Richard Brown at the Computer Science Department and Tony Skalski for providing computational support.

Appendix A

In this appendix, we evaluate the relevant one-loop sum-integrals that we need. The sum-integral is de-

fined by

$$\oint_P = \left(\frac{e^{\gamma_E} \Lambda^2}{4\pi} \right)^\epsilon T \sum_{\{P_0\}} \int \frac{d^d p}{(2\pi)^d}, \quad (A1)$$

where $d = 1 - 2\epsilon$, $P_0 = (2n + 1)\pi T + i\mu$ are the fermionic Matsubara frequencies with $n = 0, 1, 2, \dots$, μ_f is the chemical potential for flavor f , and Λ is the renormalization scale associated with the $\overline{\text{MS}}$ scheme. We first consider the sum-integral

$$I_1 = \oint_{\{P\}} \frac{1}{P^2}. \quad (A2)$$

After summing over Matsubara frequencies, we can write

$$I_1 = \frac{1}{2} \int_p \frac{1}{p} \left[1 - \frac{1}{e^{\beta(p-\mu)} + 1} - \frac{1}{e^{\beta(p+\mu)} + 1} \right]. \quad (A3)$$

The first integral in Eq. (A3) which is independent of μ and T has logarithmic divergences in the infrared and in the ultraviolet. The integral vanishes if the same scale is used in the regularization of the ultraviolet and infrared divergences [45]. If different scales are used, the value of the integral is

$$\int_p \frac{1}{p} = \frac{1}{4\pi} \left[\frac{1}{\epsilon_{\text{UV}}} - \frac{1}{\epsilon_{\text{IR}}} + \log \frac{\Lambda_{\text{UV}}^2}{\Lambda_{\text{IR}}^2} \right], \quad (A4)$$

where the subscripts UV and IR indicate the different scales. The second and third integrals in Eq. (A3) which depend on μ and T have logarithmic infrared divergences. The integrals can also be calculated in dimensional regularization and read

$$\frac{1}{2} \int_p \frac{1}{p} \left[\frac{1}{e^{\beta(p-\mu)} + 1} + \frac{1}{e^{\beta(p+\mu)} + 1} \right] = - \left(\frac{e^{\gamma_E} \Lambda_{\text{IR}}^2}{T^2} \right)^{\epsilon_{\text{IR}}} \frac{\Gamma(-2\epsilon_{\text{IR}})}{2\sqrt{\pi}\Gamma(\frac{1}{2} - \epsilon_{\text{IR}})} [\text{Li}_{-2\epsilon_{\text{IR}}}(-e^{-\beta\mu}) + \text{Li}_{-2\epsilon_{\text{IR}}}(-e^{\beta\mu})], \quad (A5)$$

where $\text{Li}_s(z)$ is the polylogarithmic function with argument z and the subscript IR indicates the dimensional regularization is used to regulate the infrared divergences. Expanding in powers of ϵ_{IR} to order ϵ_{IR}^0 yields

$$\begin{aligned} \frac{1}{2} \int_p \frac{1}{p} \left[\frac{1}{e^{\beta(p-\mu)} + 1} + \frac{1}{e^{\beta(p+\mu)} + 1} \right] = & -\frac{1}{4\pi} \left[\frac{1}{\epsilon_{\text{IR}}} + \log \frac{\Lambda_{\text{IR}}^2}{T^2} + 2\gamma_E - 2\log 2 + 2 \frac{\partial \text{Li}_{-2\epsilon_{\text{IR}}}(-e^{-\beta\mu})}{\epsilon_{\text{IR}}} \right]_{\epsilon_{\text{IR}}=0} \\ & + 2 \frac{\partial \text{Li}_{-2\epsilon_{\text{IR}}}(-e^{\beta\mu})}{\epsilon_{\text{IR}}} \Big|_{\epsilon_{\text{IR}}=0} \Big]. \end{aligned} \quad (A6)$$

Subtracting Eq. (A6) from Eq. (A4), we find

$$I_1 = \frac{1}{4\pi} \left[\frac{1}{\epsilon_{\text{UV}}} + \log \frac{\Lambda_{\text{UV}}^2}{T^2} + 2\gamma_E - 2\log 2 + 2 \frac{\partial \text{Li}_{-2\epsilon_{\text{IR}}}(-e^{-\beta\mu})}{\epsilon_{\text{IR}}} \Big|_{\epsilon_{\text{IR}}=0} + 2 \frac{\partial \text{Li}_{-2\epsilon_{\text{IR}}}(-e^{\beta\mu})}{\epsilon_{\text{IR}}} \Big|_{\epsilon_{\text{IR}}=0} \right]. \quad (A7)$$

We note that the poles in ϵ_{IR} cancel. Eq. (A7) simplifies in the case $\mu = 0$. Using $\frac{\partial \text{Li}_{-2\epsilon_{\text{IR}}}(-1)}{\epsilon_{\text{IR}}}\big|_{\epsilon_{\text{IR}}=0} = \frac{1}{2} \log \frac{2}{\pi}$, we find

$$I_1 = \frac{1}{4\pi} \left[\frac{1}{\epsilon_{\text{UV}}} + \log \frac{\Lambda_{\text{UV}}^2}{\pi^2 T^2} + 2\gamma_E \right]. \quad (\text{A8})$$

The second sum-integral we need is

$$I_2 = \oint_{\{P\}} \frac{1}{P^4}. \quad (\text{A9})$$

I_2 is finite in the infrared as well as in the ultraviolet. Integration in $d = 1$ dimension then yields

$$\begin{aligned} I_2 &= \frac{T}{4} \sum_{n=-\infty}^{n=\infty} \frac{1}{|P_0|^3} \\ &= \frac{1}{32\pi^3 T^2} \sum_{n=-\infty}^{n=\infty} \frac{1}{\left|n + \frac{1}{2} + \frac{i\mu}{2\pi T}\right|^3} \\ &= \frac{1}{32\pi^3 T^2} \left[\zeta\left(3, \frac{1}{2} + \frac{i\mu}{2\pi T}\right) + \zeta\left(3, \frac{1}{2} - \frac{i\mu}{2\pi T}\right) \right], \end{aligned} \quad (\text{A10})$$

where $\zeta(n, z)$ is the Hurwitz zeta function.

We next show that the vacuum energy is independent of b in the limit $M \rightarrow 0$. We therefore set $m_0 = M = 0$ (if m_0 is nonzero, so is M). The dispersion relation reduces to $E_{\Delta}^{\pm} = \sqrt{(p \pm b')^2 + \Delta^2}$.

After integrating over angles, we write the the one-loop cotributions to the effective potential as $V^{\text{vac}} = V_{\text{div}}^{\text{vac}} + V_{\text{fin}}^{\text{vac}}$, where

$$V_{\text{div}}^{\text{vac}} = -\frac{2N_c(e^{\gamma_E}\Lambda^2)^{\epsilon}}{\sqrt{\pi}\Gamma(\frac{1}{2}-\epsilon)} \int_0^{\infty} \sqrt{p^2 + \Delta^2} p^{-2\epsilon} dp \quad (\text{A11})$$

$$V_{\text{fin}}^{\text{vac}} = -\frac{N_c(e^{\gamma_E}\Lambda^2)^{\epsilon}}{\sqrt{\pi}\Gamma(\frac{1}{2}-\epsilon)} \int_0^{\infty} \left[\sqrt{(p+b')^2 + \Delta^2} + \sqrt{(p-b')^2 + \Delta^2} - 2\sqrt{p^2 + \Delta^2} \right] p^{-2\epsilon} dp. \quad (\text{A12})$$

Integration gives

$$V_{\text{div}}^{\text{vac}} = \frac{N_c}{2\pi} \left(\frac{e^{\gamma_E}\Lambda^2}{\Delta^2} \right)^{\epsilon} \Delta^2 \Gamma(-1+\epsilon), \quad (\text{A13})$$

$$V_{\text{fin}}^{\text{vac}} = -\frac{N_c}{\pi} b'^2, \quad (\text{A14})$$

where we have evaluated $V_{\text{fin}}^{\text{vac}}$ in $d = 1$ dimensions. The term $V_{\text{fin}}^{\text{vac}}$ is exactly equal to the subtraction term $f(0, b')$ and so V is independent of b' . After

renormalization and adding the term $f(0, \frac{1}{2}\mu_I)$, we find

$$V = \frac{N_c \Delta^2}{4G} - \frac{N_c \Delta^2}{2\pi} \left[\log \frac{\Lambda^2}{\Delta^2} + 1 \right] - \frac{N_c}{4\pi} \mu_I^2 \quad (\text{A15})$$

For $\mu_I = 0$, this result is identical to the vacuum energy (34), which is a consequence of the fact that the vacuum energy depends on the quantity $M^2 + \Delta^2$.

-
- [1] Alford, M. G., A. Schmitt, and K. Rajagopal, Rev. Mod. Phys. **80**, 1455 (2008),
 - [2] Fukushima, K., and T. Hatsuda, Rept. Prog. Phys. **74**, 014001 (2011).
 - [3] P. Fulde and R. A. Ferrell, Phys. Rev. **135**, A550, (1964).
 - [4] A. Larkin and Y. Ovchinnikov, Zh. Eksp. Teor. Fiz. **47**, 1136 (1964).
 - [5] A. W. Overhauser, Phys. Rev. Lett. **4**, 415 (1960).
 - [6] A. B. Migdal, Rev. Mod. Phys. **50**, 107 (1978).
 - [7] K. Maeda, T. Hatsuda, and G. Baym, Phys. Rev. A **87**, 021604 (2013).

- [8] M. G. Alford, J. A. Bowers, and K. Rajagopal, Phys. Rev. D **63**, 074016 (2001).
- [9] R. Anglani, G. Nardulli, M. Ruggieri, and M. Mannarelli, Phys. Rev. D **74**, 074005 (2006).
- [10] L. He, M. Jin, and P.-F. Zhuang, Phys. Rev. D **75**, 036003 (2007).
- [11] T. Kojo, Y. Hidaka, L. McLerran, and R. D. Pisarski, Nucl. Phys. A **843**, 37 (2010); *ibid* **875**, 94, (2011).
- [12] T. Kojo, R. D. Pisarski, and A.M. Tsvelik, Phys. Rev. D **82**, 074015 (2010).
- [13] M. Sadzikowski and W. Broniowski, Phys. Lett. B **488**, 63 (2000).

- [14] E. Nakano and T. Tatsumi, Phys. Rev. D **71**, 114006 (2005).
- [15] D. Nickel, Phys. Rev. D **80**, 074025 (2009).
- [16] D. Nickel, Phys. Rev. Lett. **103**, 072301 (2009).
- [17] S. Carignano, D. Nickel, and M. Buballa Phys. Rev. D **82**, 054009 (2010).
- [18] S. Carignano, M. Buballa, and B.-J. Schaefer, Phys. Rev. D **90**, 014033 (2014).
- [19] H. Abuki, Phys. Lett. B **728**, 427 (2014).
- [20] J. Braun, S. Finkbeiner, F. Karbstein, and D. Roscher Phys. Rev. D **91**, 116006 (2015).
- [21] T.-G. Lee, E. Nakano, Y. Tsue, T. Tatsumi, B. Friman, Phys. Rev. D **92**, 034024 (2015).
- [22] A. Heinz, F. Giacosa, and D. H. Rischke, Nucl. Phys. A **933**, 34 (2015).
- [23] M. Buballa and S. Carignano, Eur. Phys. J. A **52**, 57 (2016).
- [24] A. Heinz, F. Giacosa, M. Wagner, and D. H. Rischke, Phys. Rev. D **93**, 014007 (2016).
- [25] R. Anglani, R. Casalbuoni, M. Ciminale, N. Ippolito, R. Gatto, M. Mannarelli, and M. Ruggieri, Rev. Mod. Phys. **86**, 509 (2014).
- [26] M. Buballa and S. Carignano, Prog. Part. Nucl. Phys. **81**, 39 (2015).
- [27] N. D. Mermin and H. Wagner, Phys. Rev. Lett. **17**, 1133 (1966).
- [28] S. Coleman, Commun. Math. Phys. **31**, 259 (1973).
- [29] O. Schnetz, M. Thies, and K. Urlichs, Annals Phys. **321**, 2604 (2006).
- [30] M. Thies, J. Phys. A **39**, 12707 (2006).
- [31] C. Boehmer, M. Thies, and K. Urlichs, Phys. Rev. D **75**, 105017 (2007).
- [32] G. Basar, G. V. Dunne, and M. Thies, Phys. Rev. D **79**, 105012 (2009).
- [33] G. Basar and G. V. Dunne, Phys. Rev. Lett. **100**, 200404 (2008); Phys. Rev. D **78**, 065022 (2008).
- [34] D. Ebert and K. G. Klimenko, Phys. Rev. D **80**, 125013 (2009).
- [35] D. Ebert, N. V. Gubina, K. G. Klimenko, S. G. Kurbanov, and V. Ch. Zhukovsky, Phys. Rev. D **84**, 025004 (2011).
- [36] V. Ch. Zhukovsky, K. G. Klimenko, and I. E. Frolov, Moscow Univ. Phys. Bull. **65**, 539 (2010).
- [37] N. V. Gubina, K. G. Klimenko, S. G. Kurbanov, and V. Ch. Zhukovsky Phys. Rev. D **86**, 085011 (2012).
- [38] M. Thies, e-Print: arXiv:1603.06218.
- [39] P. Adhikari and J. O. Andersen, arXiv:1608.01097.
- [40] J. O. Andersen and T. Brauner, Phys. Rev. D **81**, 096004, (2010).
- [41] D. Gross and A. Neveu, Phys. Rev. D **10**, 3235 (1974).
- [42] G. Aarts, D. Ahrensmeier, R. Baier, J. Berges, and J. Serreau, Phys. Rev. D **66**, 045008 (2002).
- [43] J. O. Andersen, Phys. Rev. D **75**, 065011 (2007).
- [44] T. D. Cohen, Phys. Rev. Lett. **91**, 222001 (2003).
- [45] E. Braaten and A. Nieto, Phys. Rev. D **51**, 6990 (1995).